Revised historical Northern Hemisphere black carbon emissions based on inverse modeling of ice core records

Sabine Eckhardt[1*], Ignacio Pisso[1], Nikolaos Evangeliou[1], Christine Groot Zwaaftink[1], Andreas Plach[2], Joseph R. McConnell[3], Michael Sigl[4,5], Meri Ruppel[6,7], Christian Zdanowicz[8], Saehee Lim[9], Nathan Chellman[3], Thomas Opel[10], Hanno Meyer[10], Jørgen Peder Steffensen[11], Margit Schwikowski[12] and Andreas Stohl[2]

[1] NILU - Norwegian Institute for Air Research, Kjeller, Norway

[2] Department of Meteorology and Geophysics, University of Vienna, Austria

[3] Division of Hydrologic Sciences, Desert Research Institute, Reno, NV 89512, USA

[4] Environmental Physics, Physics Institute, University of Bern, 3012 Bern, Switzerland

[5] Oeschger Centre for Climate Change Research, University of Bern, 3012 Bern, Switzerland

[6] Atmospheric Composition Unit, Finnish Meteorological Institute, Helsinki, Finland

[7] Ecosystems and Environment Research Programme, University of Helsinki, Finland

[8] Department of Earth Sciences, Uppsala University, Uppsala, Sweden

[9] Department of Environmental Engineering, Chungnam National University, Daejeon 34134, South Korea

[10] Alfred Wegener Institute Helmholtz Centre for Polar and Marine Research, Potsdam, Germany

[11] Niels Bohr institute, University of Copenhagen, Copenhagen, Danmark

[12] Paul Scherrer Institut, Villigen, Switzerland

Correspondence to: Sabine Eckhardt (sec@nilu.no)

Abstract

Black carbon emitted by incomplete combustion of fossil fuels and biomass has a net warming effect in the atmosphere and reduces the albedo when deposited on ice and snow; accurate knowledge of past emissions is essential to quantify and model associated global climate forcing. Although bottom-up inventories provide historical Black Carbon emission estimates that are widely used in Earth System Models, they are poorly constrained by observations prior to the late 20th century. Here we use an objective inversion technique based on detailed atmospheric transport and deposition

1

27   modeling to reconstruct 1850 to 2000 emissions from thirteen Northern Hemisphere ice-core records. We find sub-

28   stantial discrepancies between reconstructed Black Carbon emissions and existing bottom-up inventories which do

29   not fully capture the complex spatial-temporal emission patterns. Our findings imply changes to existing historical

30   Black Carbon radiative forcing estimates are necessary, with potential implications for observation-constrained cli-

31   mate sensitivity.

32   **Introduction**

33   Black carbon (BC) is a fraction of carbonaceous aerosol that has a strong positive radiative forcing and can result in

34   severe health impacts at high concentrations. BC is considered to be among the most important climate forcers at the

35   global scale together with carbon dioxide and methane[12], with a present warming contribution estimated to be 0.1

36   degree relative to pre-industrial times, according to the recent Sixth Assessment report by the Intergovernmental Panel

37   on Climate Change [3]. Its climate effect is amplified when BC is deposited in snow- and ice-covered areas resulting in

38   decreased albedo and increased snow melt [3,4,5,6]. Because of its relatively short atmospheric lifetime (days to weeks),

39   BC is heterogeneously distributed in the atmosphere so the lack of global observations capable of capturing this het-

40   erogeneity means that modelling is crucial to assess atmospheric concentrations. The potential for climate change

41   mitigation through BC emissions reductions has been recognized. For the development of successful mitigation strat-

42   egies accurate historical BC emissions are crucial. However, many bottom-up emission inventories are poorly con-

43   strained by observations[1].

44   Global BC emissions are highly variable and depend on regional emission sources and policies. South Asia currently

45   suffers the world's highest BC pollution levels, which not only perturb Earth's radiative balance, but also threaten

46   human health by causing premature mortality [7]. Conversely, BC pollution in North America and Europe has been

47   decreasing in the last decades [8, 9]. These emission changes are directly linked via long-range atmospheric transport to

48   BC concentrations and deposition rates in the Arctic. Several Arctic air monitoring stations that have been operating

49   since 1989 [10] show decreasing atmospheric BC trends during recent years [11, 12].

50   Long-term constraints on past BC emissions beyond the atmospheric monitoring era can be reconstructed from natural

51   archives incorporated in lake sediments and glacier ice. While lake sediments are important archives of BC deposition

52   since they are distributed throughout terrestrial regions, interpretation is hampered by low resolution, generally high

53   dating uncertainties, and difficulties in quantitatively relating sediment records to atmospheric concentrations and

54   emissions, in part because BC transport to lake sediment sites can be both aeolian and fluvial [13,14]. Contrary to sediment

55   records, ice cores from the Greenland ice sheet and smaller mid- and high-latitude mountain glaciers and ice caps

56   provide direct, well-resolved, and well-dated records of solely atmospherically deposited BC. Similar to recent studies

57   quantifying ancient, Medieval, and modern atmospheric lead [15] and other pollutant emissions [16], ice-core records pro-

58   vide robust constraints on past BC emissions [17,18,15].

59   The first high-resolution ice-core record of BC concentrations[19] was collected from west-central Greenland covering

60   the period 1790 to 2005. It showed a large influence of BC from boreal forest fires before 1890 (hereafter referred to

61   as biomass burning (BB) BC), and that anthropogenic BC contribution peaked in the 1920s before decreasing during

the last few decades of the 20th century. Since this record was published, several other ice cores have been developed from Greenland[20–25], Arctic Canada[26], Svalbard[27,28], the continental United States[29], Russia [30], the European Alps[3132] South America[33] the Antarctic[17,34,35], the Himalayas [36] and the Tibetan Plateau [37]. These records show high interannual variability in large part because of year-to-year variability in transport and seasonal snow deposition at the coring sites, but robust multi-annual trends related to historical changes in regional emissions are clear.

Interpretation of some of these records has been underpinned by detailed atmospheric transport and deposition modeling [17,35]. Bauer et al., 2013[25] reported underestimation of modelled BC deposition for Greenland at the beginning of the 20th century and overestimation towards the end of the century. Comparisons of simulated BC deposition in aerosol transport models [38,39] with snow/ice observations revealed biases likely related to deficiencies in the underlying emission inventories. In the Arctic, significant uncertainties in historical emission inventories are related to inaccuracies in the spatial representation and high variability in emission estimates for individual source sectors[2]. High uncertainties in BC emissions are directly propagated to modelled atmospheric transport and deposition, and consequently to climate impact assessments of BC[1]. Therefore, more accurate quantification of BC emissions is fundamental for climate modelling. It is crucial to provide independent constraints on BC emissions, especially for historical emissions that are associated with the largest uncertainties because of a lack of observations. Here we use a formal inversion technique to quantitatively constrain the emissions in several broad regions based on a large array of ice-core BC records. While earlier studies have used individual ice cores to discuss implications for historical emissions [25], here we make use of an array of thirteen BC ice-core records collected from mid- to high-latitude Northern Hemispheric sites to constrain historical BC emissions since the late 19th century Industrial Revolution. BC deposition records were collected from Greenland, Arctic Canada, Russia, Svalbard, and mid- latitude glaciers in the European Alps and the Caucasus (supplementary Table S1). All the ice cores, except the Holtedahlfonna record, were analyzed using the single-particle soot-photometer method[19] so BC concentrations should be closely comparable, although there were differences in sample handling (e.g., continuous versus discrete sample measurements[40] that may have affected some of the records. Temporal resolutions vary from sub-annual (Greenland) to sub-decadal (e.g., Canada); hence, we here focus on trends in decadal-scale deposition so the effects of any dating uncertainties, sampling resolutions, or post-depositional processes should be relatively small[18]. The unprecedented size and geographic breadth of this ice-core array allows for exceptional robustness in the inferred BC emissions since BC deposition trends recorded in multiple ice cores likely reflect changes at regional to continental scales.

For each ice-core site we calculated monthly footprint emission sensitivities (FES) that allow quantification of the impact of emissions on the BC deposition at the receptor. FES is the probability that emissions occurring at any gridcell lead to deposition at the receptor. Thus, FES can be high even in regions where there are no BC emissions.

We used meteorological re-analysis data for the 20th century (Methods) for the calculations of the FES and extended our calculations back to 1850 assuming that dynamics of atmospheric transport and deposition in the 19th century were the same as in the 20th. Similar calculations have been performed to investigate historical deposition of lead in Greenland [41] and BC in Antarctica [17]. Finally, the modelled FES together with the thirteen ice core observations of BC were used in an inversion framework to quantitatively constrain emissions in several broad regions **(Methods).**

Results and Discusion

Source regions for the ice core locations

100 Results show that the northern Greenland high-altitude ice-core sites (Fig. 1a) have lower FES values overall and
101 particularly in the Arctic, reflecting the fact that air arrives at these high-altitude sites ($\geq$ 2000 m a.s.l.) via the free
102 troposphere and has less surface contact than air arriving at lower-altitude sites. Southern Greenland ice core sites
103 (Fig. 1b) are sensitive to BC emissions in North America but also in the UK and Scandinavia. The low-altitude Flade
104 Isblink site in northeastern Greenland (Fig. 1d), Devon ice cap in Canada, and the three sites in the European Arctic
105 (Fig. 1c) are more sensitive to emissions in Eurasia than to North America. In particular, the Akademii Nauk and
106 Svalbard (Fig 1c) ice core sites are highly sensitive to emissions in Russia and Northern Europe. The Colle Gnifetti
107 (Fig. 1f) and Mt. Elbrus sites (Fig 1g) are mostly sensitive to emissions in Western and Central Europe, and Eastern
108 Europe and Russia, respectively. These results show that the different ice cores receive BC emitted from different
109 source areas, but also that their FES overlap, implying that no ice core record is uniquely representative of BC emis-
110 sions from only one region. However, collectively they provide regional emission information that can be extracted
111 from the joint record.

Modelled and observed black carbon deposition fluxes

113 By combining the FES (Fig. 1) with different emission inventories we obtained modeled BC deposition fluxes at the
114 ice core sites. We did this separately for two BC emission inventories used for the 5th and 6th climate model inter
115 comparison projects (CMIP5 and CMIP6; Fig S1), which can be directly compared to observations. However, to avoid
116 biases (details below) when performing the inversion, we scaled the modelled concentration to the observations; the
117 original/unscaled values can be found in the supplement in Fig. S3. Mean observed BC deposition fluxes (Fig. 2) at
118 the various ice-core sites over the period 1850-2000 span an order of magnitude, with the lowest values at high altitude
119 Greenland sites and Devon (0.2-0.3 mg m^{-2} year) and the highest values at Mt. Elbrus (4.2 mg m^{-2} year) and Holtedahl-
120 fonna, Svalbard (12.3 mg m^{-2} year). However, the higher flux at Holtedahlfonna is most likely due to a different BC
121 quantification method used at this site, which is known to produce higher concentrations (Supplementary Data Table
122 S1), and local contamination from Svalbard coal mines has been ruled out by several previous studies [27,43]. Generally,
123 these observed differences in BC deposition fluxes between the different ice cores of about one order of magnitude
124 are reflected well in the modeled fluxes which span from 0.9 mg m^{-2} year for Tunu to 7.0 mg m^{-2} year for Mt. Elbrus
125 when using CMIP5 emissions and 0.6 mg m^{-2} year to 4.1 mg m^{-2} year with CMIP6 emissions (Fig. S3), although
126 substantial biases exist at individual sites.

127 In most Greenland ice-core records observed BC deposition peaks around 1910 and then decreases towards 2000 (Fig.
128 2). At ACT2, D4 and Summit, post-1950 fluxes are about 25% of early 20th century values, with no prominent later
129 increases. The timing of the early 20th century BC deposition maximum in Greenland ice cores is much better captured
130 by our model when using CMIP5 rather than CMIP6 emissions, suggesting that early 20th century BC emissions from
131 North America are incorrectly represented in the CMIP6 inventory. In contrast to Greenland, the Akademii Nauk and
132 Holtedahlfonna ice cores (Eurasian Arctic) and the Mt Elbrus core show rising BC deposition in the late 20th century,

133   peaking in the 1970s on Mt Elbrus and the 1980s at Akademii Nauk and Holtedahlfonna. This is consistent with
134   continuous increases in continental BC emissions at lower latitudes in Russia and Central, East and South (CES) Asia,
135   documented in both the CMIP5 and CMIP6 inventories, and which only ended in the 1980s (Fig. S1). Increasing BC
136   deposition through the late 20th century is also documented in lake sediments from north-western Arctic Russia. This
137   was attributed in part to growing BC emissions from natural gas flaring in the mainland Russian Arctic[14] which is an
138   important source region for Akademii Nauk and Holtedahlfonna (Fig. 1). Greenland ice core records (ACT2, Summit,
139   D4 and Tunu) have comparatively low BC deposition fluxes in the late 20th century, suggesting that the 1980s maxi-
140   mum in the Akademii Nauk and Holtedahlfonna ice cores is mostly due to BC emissions from the former Soviet
141   Union, which dropped in the 1980s because of the economic collapse and political disintegration. The temporal evo-
142   lution of BC emissions in the former Soviet Union is likely better represented in the CMIP6 than the CMIP5 invento-
143   ries, since there is a better agreement between the modeled and measured BC deposition fluxes in the second half of
144   the 20th century at Akademii Nauk, Holtedahlfonna and Mt. Elbrus (Fig. 2) when using the CMIP6 data.

Inversion results

146   The fact that different ice-core sites are sensitive to BC emissions from different source regions (Fig. 1) provides an
147   opportunity to use inverse modelling for constraining historical emissions with the ice-core records. This approach
148   requires the use of so-called *a priori* emissions, for which we use the average of CMIP5 and CMIP6 inventories,
149   combined with BC emission data from biomass burning (BB[44]; for emission variation see supplementary data Fig.
150   S1). We then applied a Bayesian inversion algorithm (Methods) to the decadally-averaged ice-core records of BC
151   deposition from 1850 to 2000 to determine optimized *a posteriori* BC emissions in four source regions (North Amer-
152   ica, Europe, Russia and the CES Asia; Fig. 3d, inset). A potential problem with this approach is that model biases or
153   inaccuracies in the ice-core records (e.g., age model, post-depositional snow scouring by wind or melt water percola-
154   tion) can be imprinted on the emissions retrieved by the inversion. To bypass this problem, we scaled the modeled BC
155   deposition fluxes for each ice core to the observed values of the last decade (Supplementary Data Fig. S2), on the
156   assumption that the *a priori emissions* are most reliable during that period, and that model and observational biases
157   and the representativity of the sites did not change with time. This emphasizes temporal variability and removes un-
158   certainties associated with absolute BC concentrations measured using different methods. Sensitivity studies without
159   scaling the model results to observations, show that European emissions are unrealistically low, while the other emis-
160   sions are unaffected (Supplementary Data Fig. S9).

161   The largest change between *a priori* (inventory-based) and *a posteriori* (updated after the inversion) BC emissions is
162   an increase of the emissions in North America from 1880 to 1920 (Fig. 3a). Inverse modelling suggests that BC
163   emissions there peaked higher and earlier (in the 1900s) than reported in CMIP emission inventories. Following this
164   peak, *a posteriori* emissions drop rapidly to a minimum during the Great Depression of the 1930s [45] when they reach
165   about one third of their 1900s maximum. This rapid drop in emissions is also absent in the CMIP inventories. Modeled
166   emissions in the second half of the 20th century are more consistent with the inventories. Sensitivity tests showed that
167   the results obtained for North America are robust against changes in the inversion setup (Supplementary Data Fig. S9
168   and S10).

169   For Europe, the inversion decreases the *a priori* emissions over the whole period, with the exception of the late 20th

170   century, when the emissions are nearly unchanged (Fig. 3b). The largest difference is that the *a priori* emissions start

171   to decrease in the early 1970s, whereas the *a posteriori* emissions remain stable until the late 1980s, and then decline.

172   For Russia, the modeled *a posteriori* emissions are substantially lower than those in the CMIP inventories from about

173   1900 to 1950 (Fig. 3c). The largest difference is in the 1910s, when posterior emissions are up to 65% lower. It seems

174   plausible that Russian BC emissions decreased during this time, a consequence of the turmoils of the October Revo-

175   lution and World War I, which caused the economy to collapse [46,47]. The early 20th century drop in a posteriori Russian

176   BC emissions is entirely absent in the CMIP5 and CMIP6 emission inventories, which show a continuous increase of

177   BC emissions in Russia, with little variability. Before 1900 and after 1950, *a priori* and *a posteriori* BC emissions are

178   essentially identical, and clearly show the steep decline in Russian BC emissions during the 1980s.

179   For CES Asia, *a priori* and *a posteriori* BC emissions are nearly the same (Fig. 3d). This is likely a result of the limited

180   sensitivity of BC deposition at our 13 ice-core sites to emissions from this region. This limitation could be overcome

181   in the future by including ice-core records of BC from central/northern Asia in the inversion.

182   Our results, which are based on an exceptionally robust and geographically representative ice core BC deposition

183   dataset, should be implemented to improve used emission inventory data. We were able to define amendments required

184   to emission inventories in specific areas of the Northern Hemisphere. Our findings have implications for estimates of

185   global and regional radiative forcing caused by BC emissions in the last 150 years. Specifically, early 20th century BC

186   emissions in Europe and Russia are overestimated by the existing emission inventories, whereas BC emissions in

187   North America are underestimated. For North America, our modeled *posterior* emissions are about a factor two higher

188   than the CMIP6 emissions for the period 1850-1920, and nearly a factor three higher in the 1900s. It is thus likely that

189   climate models using the CMIP inventories strongly underestimate the BC radiative forcing in the western hemisphere

190   but strongly overestimate it in the eastern hemisphere, possibly affecting global circulation. These discrepancies would

191   affect simulated surface temperatures and thus also constraints on simulated climate sensitivity[48], with consequent

192   implications for projections of future warming. Thus, future efforts should be directed to further refining existing BC

193   emissions inventories for the early 20th century to increase the reliability of climate models. Increased emissions in

194   the early 20th century might also have impacted melting of Arctic ice due to albedo changes. Since our inversions

195   suggest similar emissions during the Industrial Revolution and in the recent past, a higher melting rate seems possible

196   compared to what climate models currently assume.

197   Thus, future efforts need to be directed at further refining existing BC emission inventories to increase the reliability

198   of climate models. In this study we pinpointed weaknesses in existing emission inventories, where additional analyt-

199   ical work could be targeted.

200   **Methods**

201   BC is a highly variable mixture of carbonaceous compounds with five underlying physical properties relating to its

202   microstructure, morphology, thermal stability, solubility and light absorption [49]. Currently, there is no single instru-

203   ment that can measure all properties simultaneously and no unique, standard method has been developed for BC

204 quantification. All but one of the 13 ice core records used in this study were developed using the Single Particle Soot
205 Photometer (SP2[50]), which is sensitive to refractory, sub-micron-diameter BC particles (refractory BC, or rBC). In
206 short, ice meltwater samples are aerosolized using a nebulizer and introduced to the SP2, which measures individual
207 BC particles using laser-induced incandescence to obtain a mass concentration. This approach can be used for both
208 continuous ice core analysis[19, 17] or for discrete meltwater samples[28]. The Holtedahlfonna ice core used in this study
209 was analyzed discretely using a thermal-optical method [51] which detects a wider range of BC compounds than the SP2
210 method. Table S1 summarizes the ice core records and respective measurement methods.

211 Potential sources of uncertainties in the BC deposition fluxes include instrumental limitations (e.g., under-detection
212 of very large BC particles), dating errors (< ±5 years in some cores), post-depositional effects (e.g., wind scouring of
213 snow, melt-refreeze cycles) and spatial noise (variability in deposition across space). For cores collected in the dry
214 firn zone of Greenland, these sources of uncertainties are relatively minor, but some are poorly quantified at other
215 coring sites, and will require further study. However, it is unlikely that such uncertainties would affect BC deposition
216 trends on decadal scales that are the focus of the present study.

217 For each ice core, following standard procedures, the annual BC deposition flux (mg m^{-2} yr^{-1}) was calculated by
218 multiplying the observed BC concentrations by the estimated annual net water-equivalent accumulation. For
219 Holtedahlfonna, EC deposition was calculated by dividing the total amount of EC on a filter sample by the known
220 cross section of the ice sample and the number of years covered in one filtered ice sample [27].

221 **FLEXPART modeling**

222 As in previous studies interpreting ice core data[15,17,41], the Lagrangian particle dispersion model FLEXPART version
223 10.4 [52,53] was used to obtain footprint emission sensitivities (FES) for the ice cores. The FLEXPART runs ingested
224 meteorological input from the coupled climate reanalysis for the 20th century[54,55] (CERA-20C) of the European Centre
225 for Medium Range Weather Forecasts (ECMWF) at a resolution of 2˚ x 2˚, every 6 hours, and with 91 vertical levels.
226 For the time period of 1900-1999 we performed monthly backward simulations from each ice core location, using
227 FLEXPART's capacity to quantify FES of the deposition in backward mode[56]. As the height of the ice core locations
228 at some mountain sites (especially Colle Gnifetti and Mt. Elbrus) is severely underestimated in the CERA-20C data
229 (Table S1), the scavenging height considered for wet deposition was corrected to the real height of the topography for
230 all locations. The definition of the BC aerosol is taken from Grythe et al., 2017[57]. Similar to the widely used backward
231 mode for atmospheric concentrations [56], we obtain spatially resolved FES field [42] s on a three-dimensional grid. They
232 represent the deposition at the receptor (µg m^{-2} s) that would result from an unit emission of 1 kg s^{-1} in a respective
233 model grid cell. For the analysis we used monthly resolved footprints of the 100 years averaged over the 100-year
234 CERA-20C period, combined with emissions from 1850-2000 to get modelled deposition fluxes.

235 **Emissions**

236 For biomass burning BC emissions, we used historical emissions (1750-2015)[58]. For anthropogenic BC emissions, we
237 used two different datasets. One is the historical gridded anthropogenic emission inventory [59] used for the Coupled

238 Model Intercomparison Project (CMIP) 5[60], and the other the more recent inventory[61] used for CMIP6[62]. Both inven-
239 tories provide monthly varying emission fields covering the periods from 1850-2000 and 1750-2014, respectively, on
240 a 0.25 degree resolution. More details on the regional distribution of the two emission datasets can be found in the
241 supplementary material.

242 **Inverse modeling**

243 To reconstruct historic emissions in four regions (North America, Europe, Russia and CES Asia), we used an inversion
244 method based on a maximum a posteriori (MAP) estimate with Gaussian errors. The transfer matrix was built using
245 modeled decadal average deposition fluxes at each site based on FLEXPART simulations. For each of the fifteen
246 decades (1850-2000), the modeled deposition contributed by each emission region was rearranged into a sparse matrix
247 where emissions were considered independent of each other. The fifteen decadal values for each of the thirteen sites
248 resulted in an observation vector $\mathbf{y}$ of length 195. The source regions were aggregated into four regions resulting in a
249 control vector $\mathbf{x}$ of length 60. The corresponding transfer matrix $\mathbf{H}$ has therefore 195 rows and 60 columns. The prior
250 emission factors $\mathbf{x_0}$ (a vector of ones of length 60) multiplied by $\mathbf{H}$ yield the modeled deposition values. The cost
251 function is

252 $$(1)\ J(\mathbf{x}) = (\mathbf{y} - \mathbf{Hx})\mathbf{R}^{-1}(\mathbf{y} - \mathbf{Hx}) + (\mathbf{x_0} - \mathbf{x})\mathbf{B_0^{-1}}(\mathbf{x_0} - \mathbf{x})$$

253 where $\mathbf{R}$ and $\mathbf{B_0}$ are the error covariance matrices of the observations and the emission factors, respectively [63]; with the
254 notation of [63,64]. In both cases the off-diagonal terms were set to zero. The diagonal terms of $\mathbf{R}$ contain contributions
255 from the instrumental error of the observations $\mathbf{R_o}$ and transport model uncertainty $\mathbf{R_m}$ (we neglect other terms such as the
256 representation error due to lack of information). The diagonal terms of $\mathbf{R_o}$ are set to the mean value of the observations
257 from an assumed instrumental error of a factor two between different instrumental techniques from the literature [65].
258 The diagonal terms of $\mathbf{R_m}$ are the decadal variances of the observed values (that are affected by variability in transport).
259 The diagonal terms of $\mathbf{B_0}$ were chosen based on the magnitude of the relative difference between the CMIP5 and
260 CMIP6 emission and increase backward in time based on the assumption that earlier emissions are more uncertain
261 than more recent ones. Therefore, the relative error is 30% for the most recent decade, linearly increasing to 100% for
262 the first decade (1850-1860). The resulting posterior[63] emission factors are

263 $$(2)\ \mathbf{x} = \mathbf{x_0} + \mathbf{B_0}\mathbf{H^T}\left(\mathbf{HB_0H^T} + \mathbf{R}\right)(\mathbf{y} - \mathbf{Hx_0})$$

264

265 **Data availability**

266 Links to emission inventories: https://esgf-node.llnl.gov/search/input4mips/ (van Marle et al., 2016). https://esgf-
267 node.llnl.gov/search/input4mips/ (Hoesly et al., 2018). Meteorological data are taken from the CERA-20 project, for
268 more details www.ecmwf.int.. Ice core data can be accessed via: Flade Isblink, Akademii Nauk:
269 https://doi.org/10.18739/A2W37KX21, Humboldt, https://arcticdata.io/catalog/view/doi:10.18739/A23T9D689,
270 Tunu https://arcticdata.io/catalog/view/doi:10.18739/A2ZQ1G; Neem: Sigl, Michael; McConnell, Joseph R (2022):
271 NEEM-2011-S1 ice-core aerosol record (conductivity, NH4, NO3, BC, acidity, Na, Mg, S, Ca, Mn, Sr, Ce) in NW-

272 Greenland at 2 cm resolution from 86-1997 CE on the annual-layer counted NS1-2011 chronology. PANGAEA,
273 https://doi.org/10.1594/PANGAEA.940553; Colle Gnifetti: Sigl, Michael; Abram, Nerilie J; Gabrieli, Jacopo; Jenk,
274 Theo M; Osmont, Dimitri; Schwikowski, Margit (2018): Annual record of black carbon (rBC), bismuth, lead and
275 others from 1741 to 2015 AD from Colle Gnifetti ice core (Swiss/Italian Alps). PANGAEA,
276 https://doi.org/10.1594/PANGAEA.894785,; Mt. Elbrus: doi:10.5194/acp-17-3489-2017; The rBC data from the
277 Devon ice cap in ASCII text format through the Canadian Polar Data Catalogue: ttps://www.po-
278 lardata.ca/pdcsearch/PDCSearch.jsp?doi_id=12952 All figures were created using matlabV20b. The post-processing
279 codes can be obtained from the corresponding author upon request.

280 **Code availability**

281 The Lagrangian particle dispersion model FLEXPART is open access and FLEXPART version 10.4 is available at

282 www.flexpart.eu. The Control files used for creating the output, as well as the average emission sensitivities used for

283 the analysis can be downloaded here: https://folk.nilu.no/~sabine/BCICECORE/

284 **References**

285 1. Bond, T. C. *et al.* Bounding the role of black carbon in the climate system: A scientific assess-
286   ment. *Journal of Geophysical Research-Atmospheres* **118**, 5380–5552 (2013).

287 2. AMAP. *AMAP assessment 2015: Methane as an Arctic climate forcer. AMAP assessment report*
288   (2015).

289 3. IPCC. *Summary for Policymakers. In: Climate Change 2021*. (2021)
290   doi:10.1017/9781009157896.001. (Fig SPM.2)

291 4. Flanner, M. G., Zender, C. S., Randerson, J. T. & Rasch, P. J. Present-day climate forcing and re-
292   sponse from black carbon in snow. *Journal of Geophysical Research-Atmospheres* **112**, (2007).

293 5. Kang, S., Zhang, Y., Qian, Y. & Wang, H. A review of black carbon in snow and ice and its im-
294   pact on the cryosphere. *Earth-Science Reviews* vol. 210 103346 Preprint at
295   https://doi.org/10.1016/j.earscirev.2020.103346 (2020).

296 6. Kang, S. *et al.* Linking atmospheric pollution to cryospheric change in the Third Pole region:
297   Current progress and future prospects. *National Science Review* vol. 6 796–809 Preprint at
298   https://doi.org/10.1093/nsr/nwz031 (2019).

299 7. Lelieveld, J., Evans, J. S., Fnais, M., Giannadaki, D. & Pozzer, A. The contribution of outdoor air
300   pollution sources to premature mortality on a global scale. *Nature* **525**, 367–371 (2015).

301 8. Yang, Y. *et al.* Source Apportionments of Aerosols and Their Direct Radiative Forcing and
302   Long-Term Trends Over Continental United States. *Earths Future* **6**, 793–808 (2018).

303 9. Kutzner, R. D. *et al.* Long-term monitoring of black carbon across Germany. *Atmos Environ*
304   **185**, 41–52 (2018).

305 10. Sharma, S., Lavoue, D., Cachier, H., Barrie, L. A. & Gong, S. L. Long-term trends of the black
306   carbon concentrations in the Canadian Arctic. *Journal of Geophysical Research-Atmospheres*
307   **109**, (2004).

308   11.   Hirdman, D. *et al.* Long-term trends of black carbon and sulphate aerosol in the Arctic:
309   changes in atmospheric transport and source region emissions. *Atmos Chem Phys* **10**, 9351–
310   9368 (2010).

311   12.   Sharma, S. *et al.* A Factor and Trends Analysis of Multidecadal Lower Tropospheric Observa-
312   tions of Arctic Aerosol Composition, Black Carbon, Ozone, and Mercury at Alert, Canada. *Jour-*
313   *nal of Geophysical Research-Atmospheres* **124**, 14133–14161 (2019).

314   13.   Ruppel, M. M. *et al.* Spatial and Temporal Patterns in Black Carbon Deposition to Dated Fen-
315   noscandian Arctic Lake Sediments from 1830 to 2010. *Environ Sci Technol* **49**, 13954–13963
316   (2015).

317   14.   Ruppel, M. M. *et al.* Observed and Modeled Black Carbon Deposition and Sources in the West-
318   ern Russian Arctic 1800-2014. *Environ Sci Technol* **55**, 4368–4377 (2021).

319   15.   McConnell, J. R. *et al.* Pervasive Arctic lead pollution suggests substantial growth in medieval
320   silver production modulated by plague, climate, and conflict. *Proc Natl Acad Sci U S A* **116**,
321   14910–14915 (2019).

322   16.   Legrand, M. *et al.* Cadmium Pollution From Zinc-Smelters up to Fourfold Higher Than Ex-
323   pected in Western Europe in the 1980s as Revealed by Alpine Ice. *Geophys Res Lett* **47**,
324   (2020).

325   17.   McConnell, J. R. *et al.* Hemispheric black carbon increase after the 13th-century Maori arrival
326   in New Zealand. *Nature* **598**, 82-+ (2021).

327   18.   Rose, N. L. & Ruppel, M. Environmental Archives of Contaminant Particles. in 187–221
328   (2015). doi:10.1007/978-94-017-9541-8_9.

329   19.   McConnell, J. R. *et al.* 20th-century industrial black carbon emissions altered arctic climate
330   forcing. *Science (1979)* **317**, 1381–1384 (2007).

331   20.   McConnell, J. R. & Edwards, R. Coal burning leaves toxic heavy metal legacy in the Arctic. *Proc*
332   *Natl Acad Sci U S A* **105**, 12140–12144 (2008).

333   21.   Sigl, M. *et al.* A new bipolar ice core record of volcanism from WAIS Divide and NEEM and
334   implications for climate forcing of the last 2000 years. *Journal of Geophysical Research-At-*
335   *mospheres* **118**, 1151–1169 (2013).

336   22.   Keegan, K. M., Albert, M. R., McConnell, J. R. & Baker, I. Climate change and forest fires syner-
337   gistically drive widespread melt events of the Greenland Ice Sheet. *Proc Natl Acad Sci U S A*
338   **111**, 7964–7967 (2014).

339   23.   Zennaro, P. *et al.* Fire in ice: two millennia of boreal forest fire history from the Greenland
340   NEEM ice core. *Climate of the Past* **10**, 1905–1924 (2014).

341   24.   Grieman, M. M., Aydin, M., McConnell, J. R. & Saltzman, E. S. Burning-derived vanillic acid in
342   an Arctic ice core from Tunu, northeastern Greenland. *Climate of the Past* **14**, 1925–1937
343   (2018).

344 25. Bauer, S. E. *et al.* Historical and future black carbon deposition on the three ice caps: Ice core
345   measurements and model simulations from 1850 to 2100. *Journal of Geophysical Research-*
346   *Atmospheres* **118**, 7948–7961 (2013).

347 26. Zdanowicz, C. M. *et al.* Historical black carbon deposition in the Canadian High Arctic: a >
348   250-year long ice-core record from Devon Island. *Atmos Chem Phys* **18**, 12345–12361
349   (2018).

350 27. Ruppel, M. M. *et al.* Increase in elemental carbon values between 1970 and 2004 observed in
351   a 300-year ice core from Holtedahlfonna (Svalbard). *Atmos Chem Phys* **14**, 11447–11460
352   (2014).

353 28. Osmont, D. *et al.* An 800-year high-resolution black carbon ice core record from Lomonoso-
354   vfonna, Svalbard. *Atmos Chem Phys* **18**, 12777–12795 (2018).

355 29. Chellman, N. *et al.* Reassessment of the Upper Fremont Glacier Ice-Core Chronologies by Syn-
356   chronizing of Ice-Core-Water Isotopes to a Nearby Tree-Ring Chronology. *Environ Sci Tech-*
357   *nol* **51**, 4230–4238 (2017).

358 30. Lim, S. *et al.* Black carbon variability since preindustrial times in the eastern part of Europe
359   reconstructed from Mt. Elbrus, Caucasus, ice cores. *Atmos Chem Phys* **17**, 3489–3505 (2017).

360 31. Lavanchy, V. M. H., Gaggeler, H. W., Schotterer, U., Schwikowski, M. & Baltensperger, U. His-
361   torical record of carbonaceous particle concentrations from a European high-alpine glacier
362   (Colle Gnifetti, Switzerland). *Journal of Geophysical Research-Atmospheres* **104**, 21227–
363   21236 (1999).

364 32. Sigl, M. *et al.* 19th century glacier retreat in the Alps preceded the emergence of industrial
365   black carbon deposition on high-alpine glaciers. *Cryosphere* **12**, 3311–3331 (2018).

366 33. Osmont, D., Sigl, M., Eichler, A., Jenk, T. M. & Schwikowski, M. A Holocene black carbon ice-
367   core record of biomass burning in the Amazon Basin from Illimani, Bolivia. *Climate of the*
368   *Past* **15**, 579–592 (2019).

369 34. Pasteris, D. R., McConnell, J. R. & Edwards, R. High-resolution, continuous method for meas-
370   urement of acidity in ice cores. *Environ Sci Technol* **46**, 1659–1666 (2012).

371 35. Liu, P. *et al.* Improved estimates of preindustrial biomass burning reduce the magnitude of
372   aerosol climate forcing in the Southern Hemisphere. *Sci Adv* **7**, (2021).

373 36. Kaspari, S. D. *et al.* Recent increase in black carbon concentrations from a Mt. Everest ice core
374   spanning 1860-2000 AD. *Geophys Res Lett* **38**, n/a-n/a (2011).

375 37. Wang, M. *et al.* Black carbon deposited in Hariqin Glacier of the Central Tibetan Plateau rec-
376   ord changes in the emission from Eurasia. *Environmental Pollution* **273**, (2021).

377 38. Skeie, R. B. *et al.* Black carbon in the atmosphere and snow, from pre-industrial times until
378   present. *Atmos Chem Phys* **11**, 6809–6836 (2011).

379 39. Evangeliou, N. *et al.* Origin of elemental carbon in snow from western Siberia and northwest-
380   ern European Russia during winter-spring 2014, 2015 and 2016. *Atmos Chem Phys* **18**, 963–
381   977 (2018).

382 40. Gleason, K. E., McConnell, J. R., Arienzo, M. M., Sexstone, G. A. & Rahimi, S. Black carbon domi-
383 nated dust in recent radiative forcing on Rocky Mountain snowpacks. *Environmental Re-
384 search Letters* **17**, 054045 (2022).

385 41. McConnell, J. R. *et al.* Lead pollution recorded in Greenland ice indicates European emissions
386 tracked plagues, wars, and imperial expansion during antiquity. *Proc Natl Acad Sci U S A* **115**,
387 5726–5731 (2018).

388 42. Eckhardt, S. *et al.* Source-receptor matrix calculation for deposited mass with the Lagrangian
389 particle dispersion model FLEXPART v10.2 in backward mode. *Geosci Model Dev* **10**, 4605–
390 4618 (2017).

391 43. Zdanowicz, C. *et al.* Elemental and water-insoluble organic carbon in Svalbard snow: a syn-
392 thesis of observations during 2007-2018. *Atmos Chem Phys* **21**, 3035–3057 (2021).

393 44. van Marle, M. J. E. *et al.* Historic global biomass burning emissions for CMIP6 (BB4CMIP)
394 based on merging satellite observations with proxies and fire models (1750-2015). *Geosci
395 Model Dev* **10**, 3329–3357 (2017).

396 45. Granados, J. A. T. & Roux, A. V. D. Life and death during the Great Depression. *Proc Natl Acad
397 Sci U S A* **106**, 17290–17295 (2009).

398 46 Angus Maddison, Monitoring the World Economy, 1820-1992. Washington, DC: Organization
399 for Economic Cooperation and Development, 1995. 255 pp. ISBN 9264145494.
400 https://doi.org/10.1111/aehr.362br1, (1995).

401 47. Markevich, A. & Harrison, M. Great War, Civil War, and Recovery: Russia's National Income,
402 1913 to 1928. *Journal of Economic History* **71**, 672–703 (2011).

403 48. Fyfe, J. C., Kharin, V. v, Santer, B. D., Cole, J. N. S. & Gillett, N. P. Significant impact of forcing
404 uncertainty in a large ensemble of climate model simulations. *Proc Natl Acad Sci U S A* **118**,
405 (2021).

406 49. Petzold, A. *et al.* Recommendations for reporting 'black carbon' measurements. *Atmos Chem
407 Phys* **13**, 8365–8379 (2013).

408 50. Schwarz, J. P. *et al.* Assessing Single Particle Soot Photometer and Integrating Sphere/Inte-
409 grating Sandwich Spectrophotometer measurement techniques for quantifying black carbon
410 concentration in snow. *Atmos Meas Tech* **5**, 2581–2592 (2012).

411 51. Chow, J. C. *et al.* The dri thermal/optical reflectance carbon analysis system: description,
412 evaluation and applications in U.S. Air quality studies. *Atmospheric Environment Part A, Gen-
413 eral Topics* **27**, 1185–1201 (1993).

414 52. Pisso, I. *et al.* The Lagrangian particle dispersion model FLEXPART version 10.4. *Geosci Model
415 Dev* **12**, 4955–4997 (2019).

416 53. Stohl, A., Forster, C., Frank, A., Seibert, P. & Wotawa, G. Technical note: The Lagrangian parti-
417 cle dispersion model FLEXPART version 6.2. *Atmos Chem Phys* **5**, 2461–2474 (2005).

418 54. Patrick, L. *et al.* CERA-20C: A Coupled Reanalysis of the Twentieth Century. *J Adv Model Earth
419 Syst* **10**, 1172–1195 (2018).

420 55. Laloyaux, P. *et al.* CERA-20C: A Coupled Reanalysis of the Twentieth Century. *J Adv Model*
421   *Earth Syst* **10**, 1172–1195 (2018).

422 56. Seibert, P. & Frank, A. Source-receptor matrix calculation with a Lagrangian particle disper-
423   sion model in backward mode. *Atmos Chem Phys* **4**, 51–63 (2004).

424 57. Grythe, H. *et al.* A new aerosol wet removal scheme for the Lagrangian particle model
425   FLEXPART v10. *Geosci Model Dev* **10**, 1447–1466 (2017).

426 58. van Marle, M. J. E. *et al.* Historic global biomass burning emissions for CMIP6 (BB4CMIP)
427   based on merging satellite observations with proxies and fire models (1750-2015). *Geosci*
428   *Model Dev* **10**, 3329–3357 (2017).

429 59. Lamarque, J. F. *et al.* Historical (1850-2000) gridded anthropogenic and biomass burning
430   emissions of reactive gases and aerosols: methodology and application. *Atmos Chem Phys* **10**,
431   7017–7039 (2010).

432 60. Taylor, K. E., Stouffer, R. J. & Meehl, G. A. AN OVERVIEW OF CMIP5 AND THE EXPERIMENT
433   DESIGN. *Bull Am Meteorol Soc* **93**, 485–498 (2012).

434 61. Hoesly, R. M. *et al.* Historical (1750-2014) anthropogenic emissions of reactive gases and
435   aerosols from the Community Emissions Data System (CEDS). *Geosci Model Dev* **11**, 369–408
436   (2018).

437 62. Eyring, V. *et al.* Overview of the Coupled Model Intercomparison Project Phase 6 (CMIP6) ex-
438   perimental design and organization. *Geosci Model Dev* **9**, 1937–1958 (2016).

439 63. Tarantola, A. *Inverse Problem Theory and Methods for Model Parameter Estimation*. (Society
440   for Industrial and Applied Mathematics, 2005). doi:doi:10.1137/1.9780898717921.

441 64. Ide, K., Courtier, P., Ghil, M. & Lorenc, A. C. Unified Notation for Data Assimilation : Opera-
442   tional, Sequential and Variational (gtSpecial IssueltData Assimilation in Meteology and
443   Oceanography: Theory and Practice). *Journal of the Meteorological Society of Japan. Ser. II* **75**,
444   181–189 (1997).

445 65. Sinha, P. R. *et al.* Seasonal Progression of the Deposition of Black Carbon by Snowfall at Ny-
446   Alesund, Spitsbergen. *Journal of Geophysical Research-Atmospheres* **123**, 997–1016 (2018).

447

448 **Author contributions**

452 **Competing Interests**

453 The authors declare they have no competing interest.
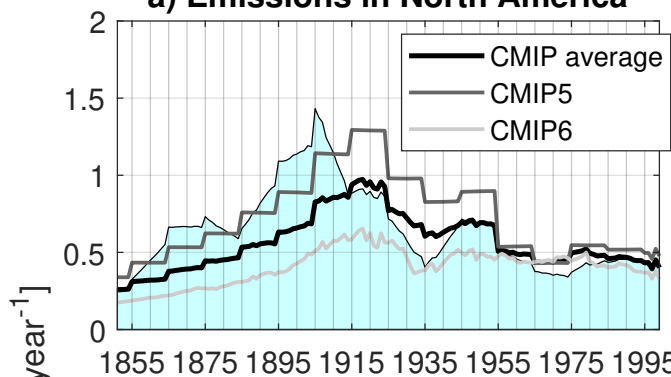
454 **Acknowledgments**

464 **Figure Legends**

465 **Fig 1. Sensitivity of black carbon deposition at Northern Hemisphere ice core sites to source region emissions.** The footprint
466 emission sensitivity (FES) in a grid cell is the simulated black carbon deposition (mg BC m^{-2} $month^{-1}$) at the ice core site that a
467 potential emission source of unit strength (1 kg s^{-1}) in that grid cell would produce [42]. It combines wet and dry black carbon
468 deposition, and accounts for black carbon source emissions below 100 m a.g.l., averaged over 100 years. The ice core sites are
469 marked with white dots. For ice core sites close to each other, FES values are averaged. We combine ice cores in the region of
470 northern Greenland (a - Summit, Tunu, NEEM, Humboldt), southern Greenland (b - ACT2, D4), three sites in the Eurasian Arctic
471 (c - Holtedahlfonna, Lomonosovfonna and Akademii Nauk), and show separately a low-altitude Greenland site (d - Flade Isblink),
472 one in the Canadian Arctic (e - Devon), and in the mid-latitudes Colle Gnifetti in the Alps (f) and Mt. Elbrus in the Caucasus (g).
473 Notice that emission sensitivity maps are combined here for display purposes only but are treated separately in the analysis.
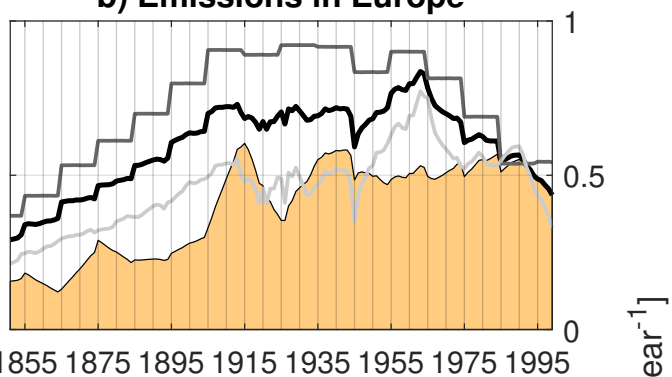
474 **Fig 2: Comparison of measured and modeled black carbon (BC) deposition fluxes for the 13 ice cores.** Observed (decadal)
475 mean annual black carbon deposition fluxes (grey) at all sites except for Holtedahlfonna, for which elemental carbon (EC) deposi-
476 tion is given with a sampling resolution of ca. 2–5 years. The *a priori* modeled values were obtained by using the biomass burning
477 emissions and the black carbon inventories for CMIP5 (light blue) and CMIP6 (dark blue), combined with monthly emission
478 sensitivities and scaled to the measured fluxes of the latest available decade. Modeled BC deposition fluxes using *a posteriori*
479 emissions from the inversion are shown with black lines. Notice that the ordinate scales are different in each panel.

480 **Fig 3: Black carbon emission history obtained from the inversion.** *A priori* (thick black line) and *a posteriori* (shaded areas)
481 emissions north of 30°N for the different regions (panels a-d). CMIP5 and CMIP6 emissions (both including the same biomass
482 burning emissions) are shown with dark and light grey lines, respectively. The regions for which the emissions are optimized are
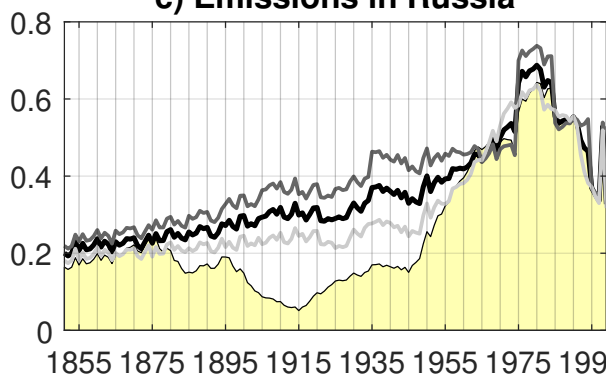483 shown as an inset in panel d and reflect the colors used in panels a to d.
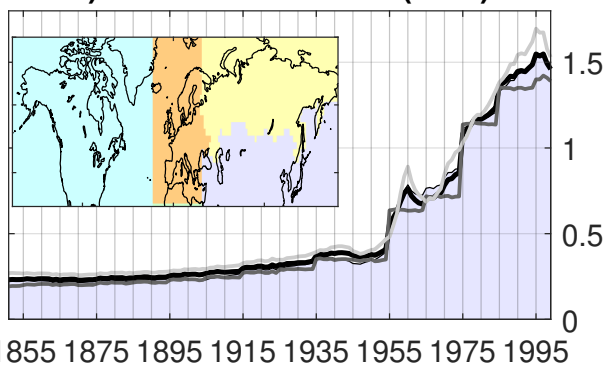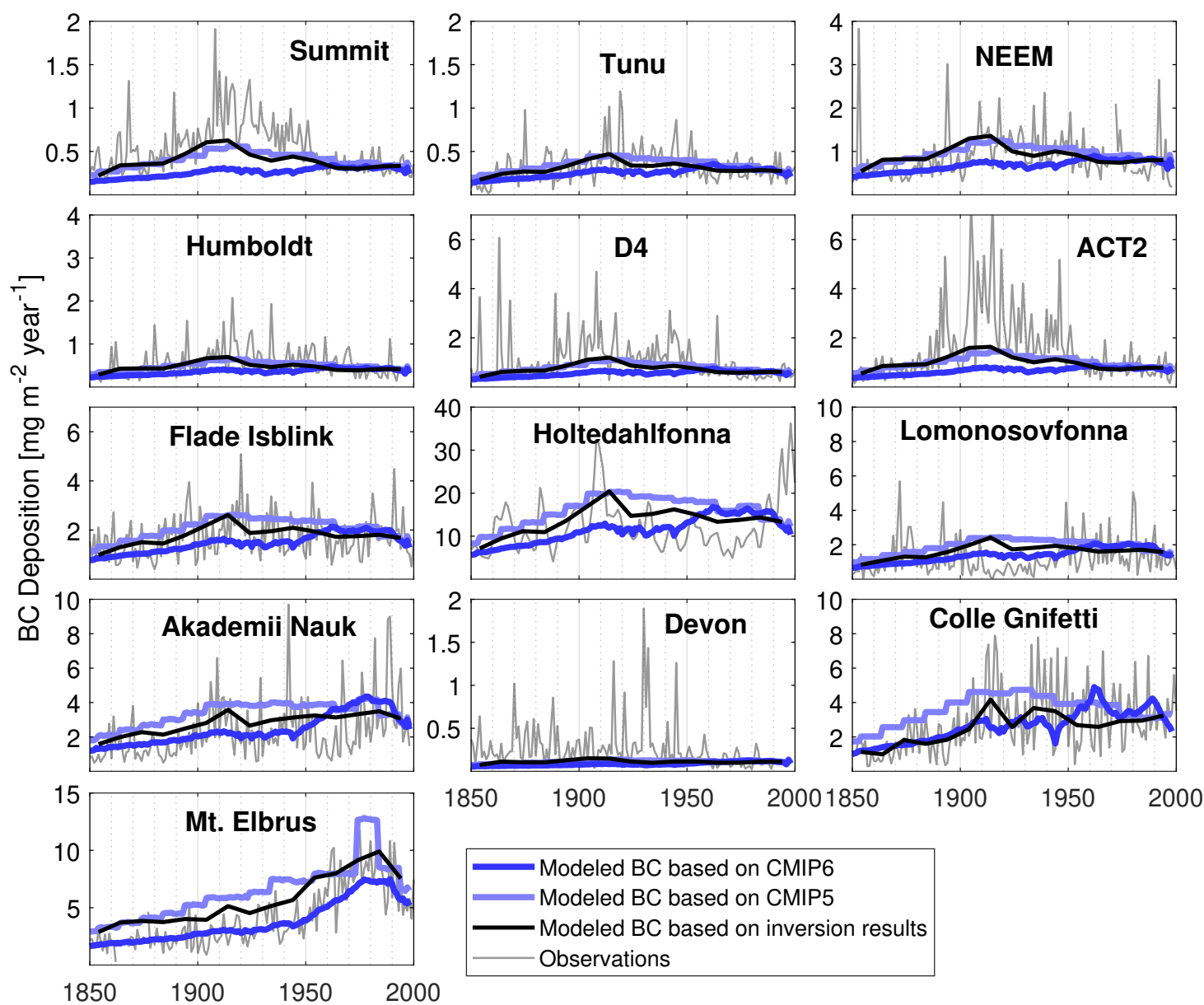
484

a) Emissions in North America
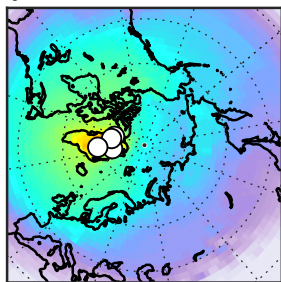
b) Emissions in Europe
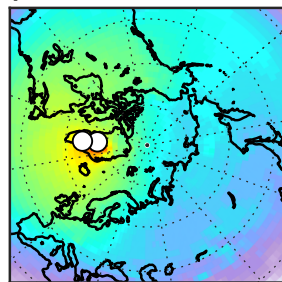
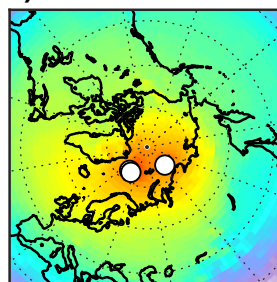**c) Emissions in Russia**

d) Emissions in Asia (CES)

— CMIP average
— CMIP5
— CMIP6

[Tg year^{-1}]

BC Deposition [mg m^{-2} year^{-1}]

Legend:
- Modeled BC based on CMIP6
- Modeled BC based on CMIP5
- Modeled BC based on inversion results
- Observations

Panels: Summit, Tunu, NEEM, Humboldt, D4, ACT2, Flade Isblink, Holtedahlfonna, Lomonosovfonna, Akademii Nauk, Devon, Colle Gnifetti, Mt. Elbrus
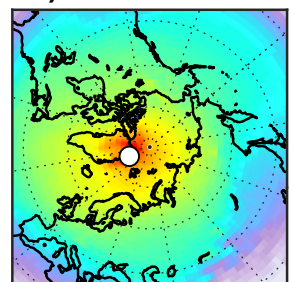
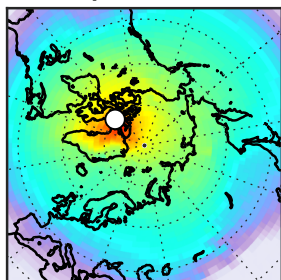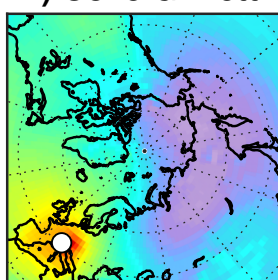a) Greenland North   b) Greenland South   c) Eurasian Arctic   d) Flade Isblink

e) Devon   f) Colle Gnifetti   g) Mt. Elbrus

2.0000
0.5000
0.1250
0.0313
0.0078
0.0020
0.0005
0.0001

(mg m^{-2} month^{-1})/(kg s^{-1})